ACS Chemical Neuroscience

Research Article

pubs.acs.org/chemneuro

Alzheimer's Amyloid-β Sequesters Caspase-3 in Vitro via Its C-Terminal Tail

Yu-Jen Chang,[†] Nguyen Hoang Linh,[‡] Yao Hsiang Shih,[†] Hui-Ming Yu,[†] Mai Suan Li,[*,§] and Yun-Ru Chen[*,†]

[†]Genomics Research Center, Academia Sinica, Taiwan, 128, Academia Road, Sec. 2, Nankang Dist., Taipei 115, Taiwan

[‡]Institute for Computational Science and Technology, SBI Building, Quang Trung Software City, Tan Chanh Hiep Ward, District 12, Ho Chi Minh City, Vietnam

[§]Institute of Physics Polish Academy of Sciences, Al. Lotnikow 32/46, 02-668 Warsaw, Poland

Supporting Information

ABSTRACT: Amyloid-β (Aβ), the main constituent in senile plaques found in the brain of patients with Alzheimer's disease (AD), is considered as a causative factor in AD pathogenesis. The clinical examination of the brains of patients with AD has demonstrated that caspase-3 colocalizes with senile plaques. Cellular studies have shown that Aβ can induce neuronal apoptosis via caspase-3 activation. Here, we performed biochemical and *in silico* studies to investigate possible direct effect of Aβ on caspase-3 to understand the molecular mechanism of the interaction between Aβ and caspase-3. We found that Aβ conformers can specifically and directly sequester caspase-3 activity in which freshly prepared Aβ42 is the most potent. The inhibition is noncompetitive, and the C-terminal region of Aβ plays an important role in sequestration. The binding of Aβ to caspase-3 was examined by cross-linking and proteolysis and by docking and all-atom molecular dynamic simulations. Experimental and *in silico* results revealed that Aβ42 exhibits a higher binding affinity than Aβ40 and the hydrophobic C-terminal region plays a key role in the caspase−Aβ interaction. Overall, our study describes a novel mechanism demonstrating that Aβ sequesters caspase-3 activity via direct interaction and facilitates future therapeutic development in AD.

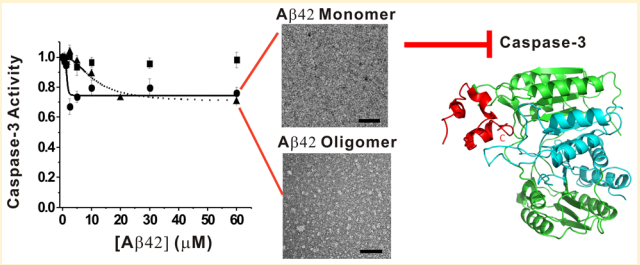

KEYWORDS: *Alzheimer's disease, amyloid-β, caspase-3, inhibition, interaction*

Alzheimer's disease (AD) is the most prevalent neurodegenerative disease among elderly people. This disease affects more than 23 million people worldwide. Two pathological hallmarks have been identified in the brain of patients with AD. They are extracellular senile plaques composed mainly of amyloid-β (Aβ) fibrils and intracellular neurofibrillary tangles, which mainly comprise hyperphosphorylated tau, a microtubule-associated protein. Aβ is a peptide with molecular mass approximately 4 kDa, generated from β- and γ-secretase cleavages of amyloid precursor protein (APP).[1] The two main isoforms are Aβ40 and Aβ42, composed of 40 and 42 amino acids (aa), respectively. They differ in the C-terminus as a result of γ-secretase cleavages and trimming.[2] Aβ is intrinsically disordered, and its aggregation is highly associated with the pathogenesis of AD. Aβ fibrillization follows a nucleation polymerization mechanism to form mature fibrils with cross-β spines. Aβ oligomers, which are prefibrillar intermediates, are considered to be the most toxic species correlated with disease progression.[3]

Monomeric Aβ is intrinsically disordered without defined secondary structures. Nevertheless, previous studies have shown the protein stability of Aβ40 and Aβ42 examined by chemical denaturation[4] and revealed a protease-resistant core ranging from residues 21 to 30[5] and residual β-strands from aa 17 to 21 and 31 to 36, connected by a turn/bend-like region at residues 20−26.[6] C-terminal Aβ residues are more hydrophobic, and short C-terminal peptides can inhibit Aβ-induced toxicity.[7] In the structural models of Aβ fibrils and oligomers, the N-terminus of Aβ ranging from residues 1 to 10 is flexible.[8] The residues 10−20 and 30−40 form in-register cross β-spines in mature Aβ40 fibrils with a salt bridge between D23 and K28,[8b] whereas Aβ42 fibrils are composed of three β-sheets, aa 12−18, 24−33, and 36−40, in which K28 forms a salt bridge with A42.[9]

Neuronal death in AD is believed to be attributed to apoptosis that involves caspase signaling and DNA fragmentation. Fragmented DNA has been found in the hippocampal and entorhinal areas of the brains of patients with AD.[10] Increased apoptotic protein Bcl-2 has been found in AD tissues.[11] Furthermore, synthetic Aβ activates apoptotic pathways in cultured hippocampal neurons[12] and evokes apoptotic reactions.[13] Caspases are cysteine-dependent and aspartate-

Received: February 18, 2016
Accepted: May 26, 2016
Published: May 26, 2016

DOI: 10.1021/acschemneuro.6b00049
ACS Chem. Neurosci. 2016, 7, 1097−1106

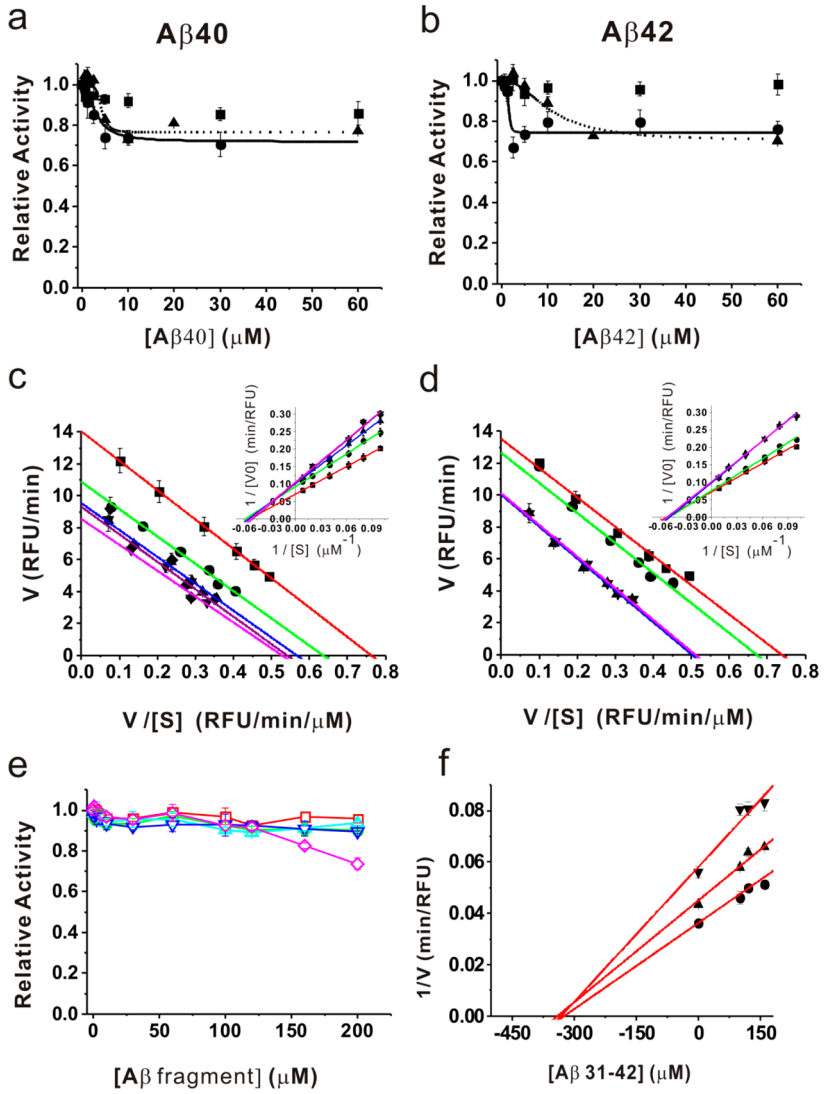

Figure 1. Inhibition of caspase-3 by Aβ40 and Aβ42 conformers. The enzyme activity of caspase-3 was measured for 1 h, and V_0 of each reaction mixed with different conformers of Aβ40 (a) and Aβ42 (b) was calculated and plotted. Freshly prepared Aβ (●), oligomer (▲), and fibril (■) were mixed with caspase-3 solution before the fluorescent substrate was added. At least three individual experiments were performed and standard deviations are shown. Data were fitted to obtain IC_{50} values and are shown in solid lines for freshly prepared Aβ and dotted lines for Aβ oligomers. (c, d) Eadie−Hofstee plot of caspase-3 activity inhibited by Aβ monomer. Initial velocity of caspase-3 was measured in the presence of various substrate concentrations (120, 50, 25, 16, 12.5, and 10 μM) with and without Aβ treatment. (c) Caspase-3 inhibited by freshly prepared Aβ40. Caspase-3 was mixed with 60 (♦, purple line), 10 (▼, magenta line), 5 (▲, blue line), and 2.5 (●, green line) μM freshly prepared Aβ40 and without Aβ40 (■, red line). (d) Caspase-3 inhibited by freshly prepared Aβ42. Caspase-3 was mixed with 10 (▼, magenta line), 5 (▲, blue line), and 1.25 (●, green line) μM of Aβ42 and without Aβ42 (■, red line). The lines are linear fits to the data. Lineweaver−Burk plots are shown in the insets. (e) Inhibition of caspase-3 by Aβ peptide fragments. The enzyme activity of caspase-3 was measured by calculating V_0 of each reaction mixed with Aβ1−15 (□, red), Aβ16−20 (○, green), Aβ21−30 (△, cyan), Aβ31−40 (▽, blue), and Aβ31−42 (◊, magenta) fragments. (f) K_i of Aβ31−42 to caspase-3. Caspase-3 activity was measured in the presence of various concentrations of Aβ31−42 (160, 120, 100, and 0 μM) and each experiment was performed under 100 (●), 50 (▲), and 25 (▼) μM of caspase-3 substrate. The lines represent linear fittings of each group. K_i value was calculated and averaged from intercepts of x-axis.

directed proteases that recognize and cleave substrates at specific aspartic residues in a protein sequence of DXXD. Upstream caspases, caspase-8 or -9, activate downstream caspases, such as caspase-3 and -7, and further degrade various cellular proteins. Caspase-3 is the major executioner in apoptosis. It exists in a zymogen form with an N-terminal pro-domain and then autoproteolyzes to form a mature caspase-3 comprising two p17 and p12 subunits. The maturation process involves cleavages of the prodomain and linkers in procaspase-3 and results in the formation of active caspase-3. Aside from apoptosis, caspase-3 also plays non-apoptotic roles in synaptic plasticity and neurodegeneration.[14]

Emerging evidence revealed that Aβ originates from intracellular space[15] in which intracellular Aβ is identified in neurons of brain tissues examined through AD neuropathology.[15a] Aβ42 is considered as the dominant intracellular Aβ species[16] and can be found in multivesicular bodies in neurons.[15a,17] It was shown that accumulation of intracellular Aβ in the hippocampus and amygdala is correlated with the early cognitive impairment in 3xTg-AD mice[18] and increase in intracellular Aβ precedes Aβ deposition in AD brains.[19] The

DOI: 10.1021/acschemneuro.6b00049
ACS Chem. Neurosci. 2016, 7, 1097−1106

production of intracellular Aβ is suggested to be from APP processing in the endoplasmic reticulum and trans-Golgi network aside from that on plasma membrane and in endosomes. Reuptake of extracellular Aβ has also been demonstrated.[15a] Interestingly, a neuroprotective role of Aβ42 monomer has been described.[20]

Recently, Aβ fibrils were shown to foster procaspase-3 maturation.[21] A cosedimentation experiment *in vitro* has demonstrated that procaspase-3 and caspase-3 colocalize with Aβ40 fibrils and synthetic or natural fibrils can serve as a platform to locally concentrate procaspase-3 for maturation. The work provides evidence that fibrillar Aβ interacts with procaspase-3 and caspase-3. On the basis of the discovery of intracellular Aβ and Aβ-induced apoptosis in AD, here, we examined the direct effect of Aβ on mature caspase-3 by using *in vitro* biochemical and *in silico* methods. We found that Aβ conformers elicit inhibitory effects on caspase-3 *in vitro*. The molecular interaction was examined by cross-linking and limited proteolysis and by docking and all-atom molecular dynamic (MD) simulations. Consistent with *in vitro* experimental results, our findings revealed that caspase-3 is predominantly bound to the C-terminus of Aβ and Aβ42 exhibits stronger binding affinity than Aβ40. The binding regions were also revealed.

RESULTS AND DISCUSSION

Aβ Conformers Inhibit Caspase-3 Activity with Freshly Prepared Aβ42 as the Most Potent Species. To understand the possible direct effect of Aβ on caspase-3, we initiated the study to examine caspase-3 activity under the treatment of different Aβ40 and Aβ42 conformers, namely, freshly prepared Aβ, Aβ oligomers, and Aβ fibrils. Different Aβ species were prepared following previous literature procedures[22] and the morphology of freshly prepared species, oligomers, and fibrils was examined by transmission electron microscopy (TEM) (see Supplementary Figure S1). We found few aggregates in the freshly prepared Aβ40 and Aβ42. By contrast, we detected many spherical oligomers and fibrils after the oligomer and fibril preparation, respectively. We first mixed active recombinant human caspase-3 with different Aβ conformers at 0.625, 1.25, 2.5, 5, 10, and 30 μM, and added the substrate to initiate the enzymatic reactions right before the measurement. The measurement was conducted for 1 h. The initial velocity, V_0, of caspase-3 was obtained and calculated from the fluorescence signal of the cleaved substrate, z-DEVD-AFC. To our surprise, we found that Aβ conformers, especially the freshly prepared species and oligomers, were able to inhibit ∼22−30% of caspase-3 activity in the micromolar range (Figure 1a,b). The activity was quantified by the initial slope of AFC fluorescence generated from the cleaved substrate, z-DEVD-AFC. When the inhibition effect of different Aβ species was compared, the freshly prepared Aβ species was found to be the most effective species to inhibit caspase-3. The 30% inhibition was reached at 5 μM for the freshly prepared Aβ40 and 2.5 μM for the freshly prepared Aβ42. Aβ oligomers could inhibit ∼22−30% of caspase-3 activity at 10 μM for Aβ40 and 20 μM for Aβ42. However, we cannot rule out that this inhibition may be a result of existing monomers in the oligomer preparation. The Aβ40 fibrils only inhibit ∼10% of caspase-3, and Aβ42 fibrils did not show significant caspase inhibition. IC_{50} values obtained from nonlinear regression data fitting were ∼2.21 ± 0.25 and ∼1.49 ± 0.39 μM for the freshly prepared Aβ40 and Aβ42, respectively, and ∼4.25 ± 1.70 and ∼25.23 ± 1.32 μM for Aβ40 and Aβ42 oligomers, respectively. To eliminate possible quenching effect of Aβ on AFC, we directly examined the fluorescence emission of AFC acrylamide in the presence of various freshly prepared Aβ40 and Aβ42 concentrations (see Supplementary Figure S2). We found that AFC fluorescence was not affected by high concentration of Aβ confirming that caspase-3 is indeed inhibited by Aβ species. We further measured the caspase-3 activity in the presence of aprotinin (6.5 kDa) or ribonuclease A (RNase A, 13.7 kDa) (see Supplementary Figure S3). None of the peptides or proteins could significantly inhibit caspase-3. Meanwhile, we examined Aβ effect on other enzymes. Both Aβ40 and Aβ42 were unable to inhibit other enzymes, such as β-glucosidase and α-galactosidase (see Supplementary Figure S4). The cell-based caspase-3 activity assay also revealed that the caspase-3 activity was significantly inhibited when the treated Aβ remained in the reaction buffer (see Supplementary Figure S5a). In contrast, when Aβ was removed from the cell culture media before substrate addition to trigger the enzymatic reaction, the caspsase-3 activity increased (see Supplementary Figure S3b). To further demonstrate that Aβ and caspase-3 colocalize in cellular space, we employed double immunofluorescence staining for intracellular Aβ and active caspase-3 in the retrosplenial cortex of 7-month-old 3xTg mice, which overexpress human APP Swedish mutation, Psen1 M146V, and Tau P301L. We clearly observed colocalization of active caspase-3 and Aβ in neurons with intact morphology (see Supplementary Figure S6). Therefore, our results demonstrated that Aβ could specifically sequester caspase-3 activity. Among the Aβ species, the freshly prepared Aβ is more potent than oligomers; conversely fibrils elicit a marginal effect.

Aβ Is a Noncompetitive Inhibitor of Caspase-3. To further understand whether Aβ inhibition on caspase-3 is competitive, we performed inhibition assays with various substrate concentrations. We used freshly prepared Aβ40 and Aβ42 as inhibitors to examine caspase-3 activity. Six different substrate concentrations were added to the caspase-3 solution, and the initial velocity, V_0, was calculated. Values of V_0 of caspase-3 and the substrate in the presence of various Aβ40 and Aβ42 concentrations were plotted in Eadie−Hofstee plot (Figure 1c,d) and Lineweaver−Burk plot (Figure 1c,d, insets). According to Michaelis−Menten equation, we found that Aβ did not affect K_m value of caspase-3 but only affected V_0. A summary of V_0 and K_m is listed in Table 1. This characteristic is consistent with the classic mechanism of noncompetitive inhibition. We combined the data from several concentrations of Aβ and found that the inhibition was saturated at 10 μM for Aβ40 (Figure 1c, magenta line) and 5 μM for Aβ42 (Figure 1d,

Table 1. V_0 and K_m Values of Caspase-3 Calculated from Figure 1c,d

inhibitor	concn (μM)	V_0 (min^{-1})	K_m (μM)
Aβ40	0	14.0 ± 0.02	18.4 ± 0.04
	2.5	10.9 ± 0.3	17.1 ± 1.0
	5	9.5 ± 0.1	16.9 ± 0.5
	10	8.5 ± 0.6	16.2 ± 2.1
	60	9.3 ± 1.1	17.2 ± 4.0
Aβ42	0	13.5 ± 0.4	18.3 ± 1.1
	1.25	12.6 ± 0.5	18.8 ± 1.5
	5	10.0 ± 0.3	20.0 ± 1.3
	10	10.1 ± 0.2	19.8 ± 0.9

DOI: 10.1021/acschemneuro.6b00049
ACS Chem. Neurosci. 2016, 7, 1097−1106

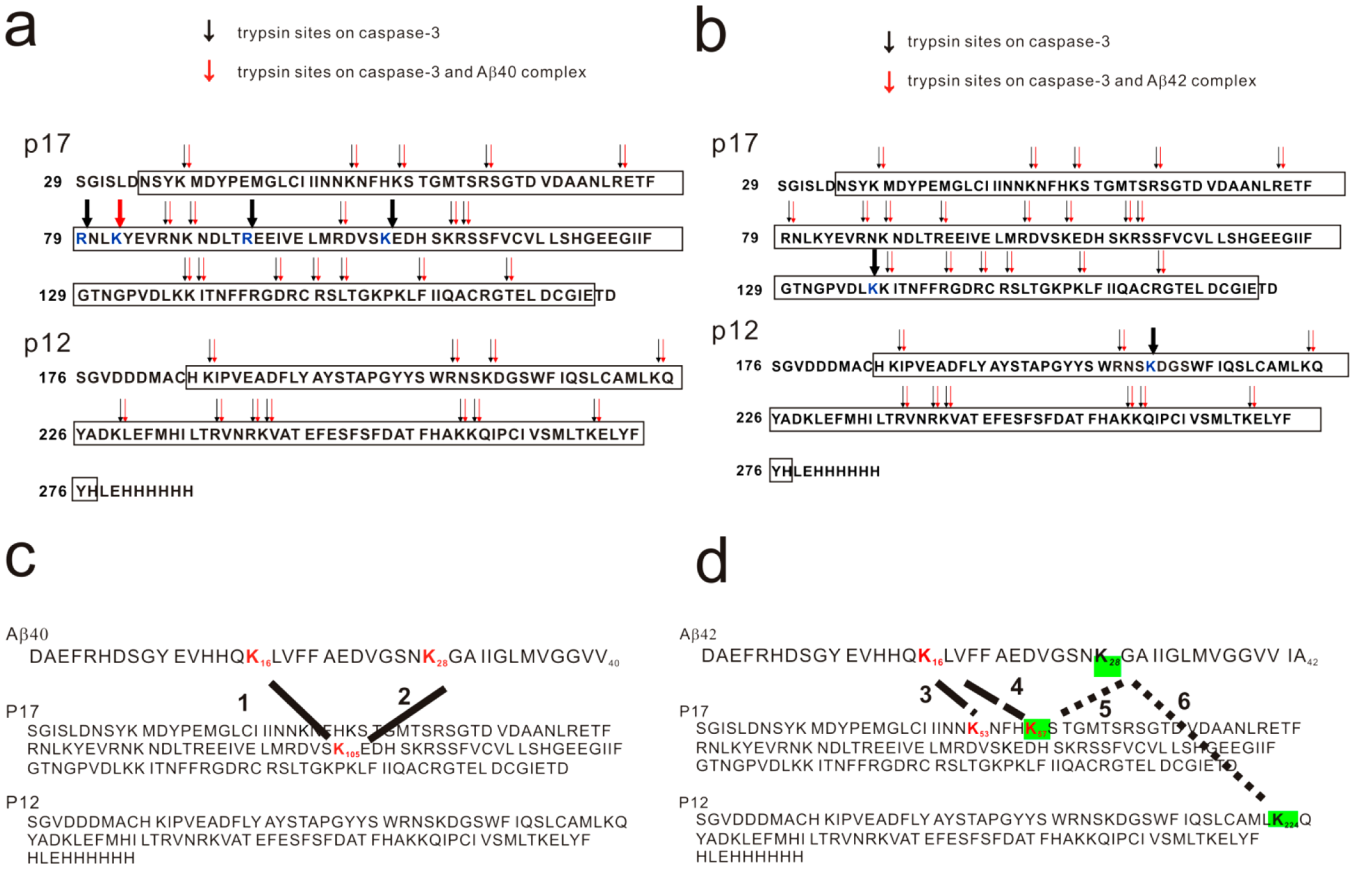

Figure 2. Proteolysis of caspase-3 mixed with Aβ40 and Aβ42. Caspase-3 was mixed with freshly prepared (a) Aβ40 or (b) Aβ42 and subjected to trypsin digestion. The residues within the subunits are boxed. All cleavage sites are indicated by arrows. The thin arrows represent the same trypsin cutting sites found in the absence (black arrows) and presence of Aβ (red arrows). The thick arrows highlight the cutting sites that are different in the absence (black arrows) and presence Aβ (red arrows). The residues at the differential cleavage sites are labeled in blue. (c, d) Cross-linked sites between caspase-3 and Aβ40 and between caspase-3 and Aβ42. Caspase-3 was mixed with freshly prepared (c) Aβ40 or (d) Aβ42, followed by BS3 cross-linking, and subjected to trypsin digestion. The digested peptides were detected by ESI-MS-MS and analyzed with MassMatrix. The linkages and cross-linked sites are illustrated by solid, dashed, and dotted lines.

blue line). These findings are similar to the results of the activity assay.

The C-Terminal Aβ42 Fragment Contributes to Caspase-3 Inhibition. To further understand Aβ contribution to caspase-3 inhibition, we used various Aβ peptide fragments to examine the inhibition (Figure 1e). Five different Aβ fragments were synthesized and examined following our previous procedure. The peptides were residues 1−15 (denoted as Aβ1−15), 16−20 (denoted as Aβ16−20), 21−30 (denoted as Aβ21−30), 31−40 (denoted as Aβ31−40), and 31−42 (denoted as Aβ31−42). We found that caspase-3 was not inhibited when the peptide concentration was below 100 μM, while full-length Aβ can show ∼30% inhibition as shown in Figure 1a,b. However, after Aβ concentration was increased to 160 μM, Aβ31−42, but not the others, showed significant inhibition of caspase-3 to approximately ∼30% inhibition. We performed the inhibition under various concentrations of Aβ31−42 and substrate. The K_i value of Aβ31−42 was calculated to be 332.1 ± 8.2 μM (Figure 1f). The result showed that the C-terminal tail of Aβ42 spanning Aβ31−42 contributed to caspase-3 inhibition to the highest extent.

The Binding Regions of Caspase-3 to Aβ40 and Aβ42 Are Distinct. To examine the interaction, we used liquid chromatography−tandem mass spectrometry (LC/MS/MS) coupled with trypsin digestion with and without cross-linking to locate the binding sites of caspase-3 and Aβ. First, we separately tryptic digested caspase-3 alone and caspase/Aβ complex and subjected the peptides to LC/MS/MS. The trypsin digestion sites were identified in many lysine (K) and arginine (R) residues in the large (p17) and small (p12) subunits of caspase-3. Caspase-3 residues were numbered in accordance with the Protein Data Bank (PDB) file 1CP3, in which p17 spans from residue 35 to 173 and p12 spans from residue 185 to 277. The Aβ40 binding to caspase-3 hindered trypsin cutting at R79, R93, and K105 of p17 and generated a new cutting site at K82 (Figure 2a). By contrast, the Aβ42 binding hindered trypsin cutting at K137 of p17 and K210 of p12 (Figure 2b). The result showed that Aβ binding may prevent tryptic digestion in the interacting region or induce conformational changes and expose new cutting sites on caspase-3. We also performed chemical cross-linking and subjected caspase-3 and Aβ complex to tryptic digestion and LC/MS/MS. The cross-linking sites were revealed after data analysis. The results showed that K16 and K28 of Aβ40 was cross-linked to K105 of p17 (linkages 1 and 2, respectively) (Figure 2c). In the case of Aβ42, K16 of Aβ42 cross-linked to K53 and K57 of p17 (linkages 3 and 4, respectively) and K28 of Aβ42 linked to K57 of p17 (linkage 5) and K224 of p12 subunit (linkage 6) (Figure 2d). The fragmentation mass spectra of the cross-linked peaks are shown in Supplementary

DOI: 10.1021/acschemneuro.6b00049
ACS Chem. Neurosci. 2016, 7, 1097−1106

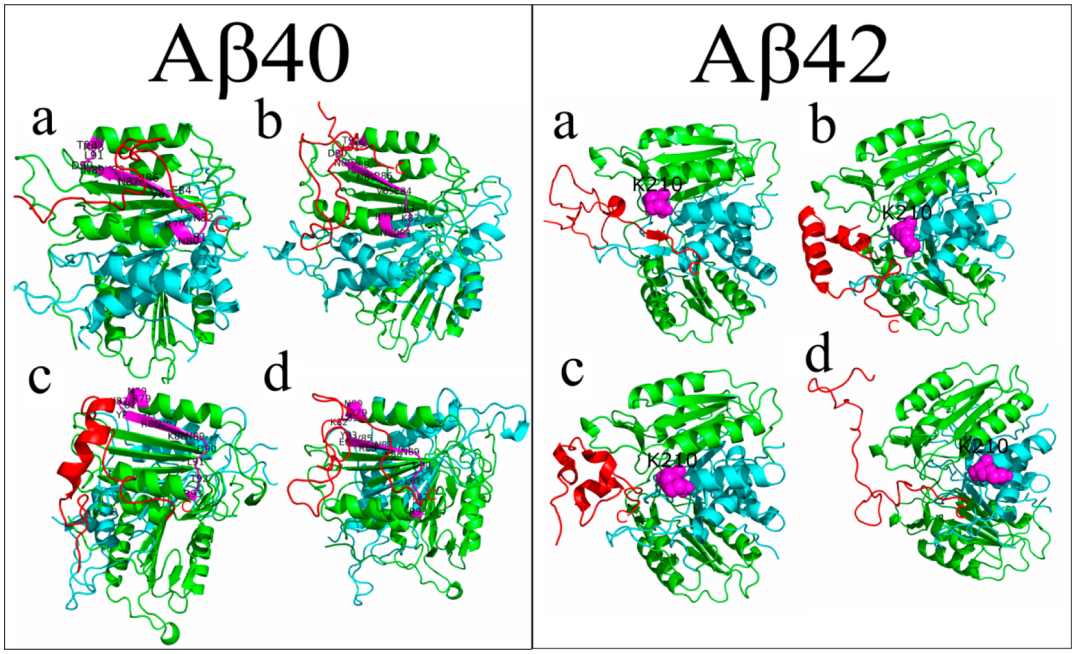

Figure 3. Best docking poses of the four representative Aβ40 and Aβ42 structures to caspase-3. The two p17 subunits are in shown green and p12 subunits are in cyan. Aβ peptides are highlighted in red. The active residues of caspase-3 that were determined by the cross-linking experiment are in magenta. In Aβ40 case, the active residues of caspase-3 are in the fragment R79−R93 of p17. In Aβ42, the active residue is K210 of p12. Panels a, b, c, and d are the best docking modes of the corresponding structures of Aβ peptides shown in supplementary Figure S8 in Supporting Information. The docking of Aβ was carried out to simulate the active regions of caspase-3. The structures shown in this figure were chosen as the initial structures for MD simulations.

Table 2. MM-PBSA Binding Free Energy of Caspase−Aβ Complexes[a]

	structure	ΔE_{elec}	ΔE_{vdW}	ΔG_{PB}	ΔG_{sur}	$-T\Delta S$	ΔG_{bind}
Aβ1−40	traj 1	−255.9	−38.8	77.1	−12.2	68.6	−161.2
	traj 2	−259.0	−25.4	81.0	−13.0	63.5	−143.1
	traj 3	−306.8	−24.2	104.9	−11.0	64.8	−163.9
	traj 4	−352.9	−34.9	175.3	−5.2	66.3	−150.6
	average	−293.5	−30.8	109.6	−10.3	65.8	−154.7 ± 9.7
Aβ1−42	traj 1	−402.3	−114.3	161.4	−13.4	83.6	−285.0
	traj 2	−422.2	−69.1	169.8	−6.4	84.6	−243.3
	traj 3	−337.8	−84.7	129.7	−10.3	91.5	−211.6
	traj 4	−411.8	−112.5	167.9	−13.5	73.3	−296.7
	average	−393.5	−95.2	157.2	−10.9	83.2	−259.2 ± 39.1

[a]All quantities are measured in kcal/mol. Results were obtained from four MD trajectories starting from the four initial conformations shown in Figure 3.

Figure S7. The results revealed distinct interacting sites of Aβ40 and Aβ42 to caspase-3.

***In Silico* Docking Study Showed That Caspase-3 Mainly Interacts with the C-Terminal Region of Aβ and Aβ42 Binds to Caspase-3 More Strongly than Aβ40.** To further examine the molecular interaction between Aβ and caspase-3, we used the HADDOCK server to dock 14 $A\beta_{40}$ structures and 25 $A\beta_{42}$ structures to caspase-3 (PDB 1CP3) (see Supplementary Figure S8). Aβ was docked to the caspase-3 regions where active residues are located, as described in Methods. By averaging the best docking structures, we obtained the mean binding energy ΔE_{bind}= −25.6 ± 16.7 and −53.7 ± 15.2 kcal/mol for Aβ40 and Aβ42, respectively. The results suggested that Aβ42 binds to caspase-3 more strongly than Aβ40 does. Figure 3 illustrates the structures obtained in the best docking mode of four representative structures denoted as a, b, c, and d (also in Supplementary Figure S8). Aβ40 peptides are predominantly located near the binding site (magenta) in the p17 subunit. Aβ42 peptides are positioned near both p17 and p12 subunits, but the region around K210 of the p12 subunit is the most crucial.

To deepen understanding of the role of the C-terminal region in complex stability, we examined hydrogen bonds (HBs) and side chain (SC) contacts. Of the representative structures obtained in the best docking mode, one structure contained 3 HBs and 11 SC contacts of Aβ40 and 6 HBs and 10 SC contacts of Aβ42 (see Supplementary Figure S9). The number of HBs is less than the number of SC contacts. This result is also valid in other systems. Thus, we focused on SC contacts because they likely play a more important role than HBs. We calculated the per-residue number of the SC contacts between Aβ peptides and caspase-3 by using the lowest energy conformation obtained in the lowest energy level (see Supplementary Figure S10). The average data of all representative structures are consistent with the experimental data. The result showed that the residues from the C-terminal

DOI: 10.1021/acschemneuro.6b00049
ACS Chem. Neurosci. 2016, 7, 1097−1106

region comprised more SC contacts with caspase-3, and this effect is more pronounced for Aβ42 compared with Aβ40.

Considering that the predictive power of the protein−protein docking method is limited because of omission of protein dynamics, we conducted additional molecular dynamic (MD) simulations to estimate the binding free energy by using the more precise MM-PBSA method and to double check other docking results. However, the MD simulation is more time-consuming than the docking simulation; as such, we restricted our study to four representative caspase−Aβ40/Aβ42 complexes. The simulation started from the best docking poses shown in Figure 3. The systems reached equilibrium at different time scales when root-mean-square displacement (RMSD) was saturated (see Supplementary Figure S11). The snapshots collected in the last 20 ns were used to compute all relevant quantities, including the binding free energy obtained by the MM-PBSA method. In the whole system, electrostatic interaction dominates over van der Waals (vdW) interaction (Table 2) presumably because Aβ peptides exhibit a net charge of −3e, whereas caspase-3 yields a net charge of +8e.

Since Aβ42 is more hydrophobic than Aβ40 due to the last two nonpolar residues, Ile41 and Ala42, the vdW interaction of Aβ42 is stronger than that of Aβ40. The entropy term is not sensitive to MD trajectories, but the entropy change of Aβ42 is larger than that of Aβ40. The finding suggests that the latter is less flexible in the Aβ/caspase-3 complex. This result is qualitatively consistent with that of the trypsin digestion experiment, in which caspase has more active residues in interaction with Aβ40 than Aβ42. Similar to protein−small ligand complexes,[23] nonpolar contributions ΔG_{sur} are minor and not sensitive to initial structures of both Aβ peptides (Table 2). In contrast, polar term ΔG_{PB} substantially depends on MD trajectories, but the difference between them is compensated by ΔE_{elec} contributions.

In agreement with our *in vitro* results, the simulation results showed that Aβ42 binds to caspase-3 more strongly than Aβ40 and Aβ42 exhibits lower binding free energy (Table 2). Prior studies revealed that short peptides that are good binders to Aβ fibrils have binding free energy per residue of about −3 kcal/mol.[24] In our study, the per-residue binding energy to caspase-3 is −154.7/40 = −3.85 kcal/mol for Aβ40 and −259.2/42 ≈ −6.17 kcal/mol for Aβ42, suggesting that the binding affinities in both cases are high.

Using the snapshots collected in equilibrium from four MD runs, we calculated the mean SC contacts per residue of Aβ (Figure 4). Similar to the docking results, we found that the C-terminal region contains more contacts than other regions, and this effect is the same in both peptides. Residues 28, 29, 31, and 37 are the most active in Aβ_{40}, while the contribution from residues 28, 36, 37, 38, 40, and 42 is dominant in the case in Aβ_{42}. The crucial role of the C-terminal region in complex stability is anticipated because the hydrophobic residues from this end prefer to stay close to caspase-3; as a result the hydrophilic N-terminus is exposed to water. The key role of the C-terminal region is verified by the result observed in HBs (see Supplementary Figure S12). The important role of the C-terminal region is also supported by the results in Figure S13 in Supporting Information, which shows the SC contact map between Aβ peptides and caspase-3. The SC contact population does not exceed 0.35 and 0.6 in Aβ40 and Aβ42, respectively. The higher population of Aβ42 is in accordance with its higher binding affinity than Aβ40.

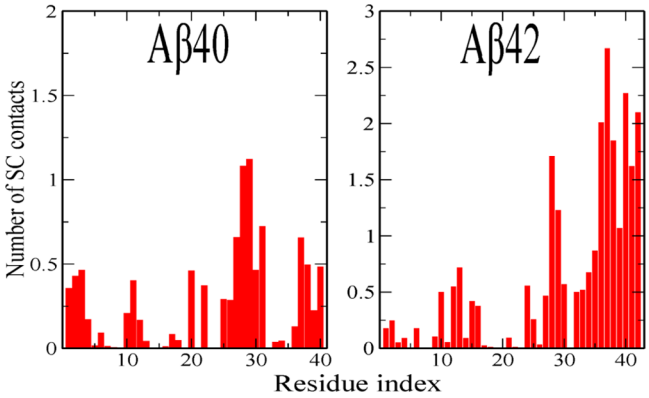

Figure 4. Per-residue number of side chain contacts between Aβ peptides and caspase-3. The results obtained in MD simulations were averaged over four trajectories.

The Most Active Caspase Residues Are Revealed by MD Results. Next, we calculated the per-residue populations of caspase-3. In a given snapshot, a residue comes in contact with Aβ when it contains at least one SC contact with any residue of the Aβ peptide. Then the per-residue distribution is defined as the number of snapshots in which a given residue of caspase comes in contact with Aβ divided by the total number of the collected snapshots in equilibrium. The results are shown in Figure 5. We assumed that the populations of the active

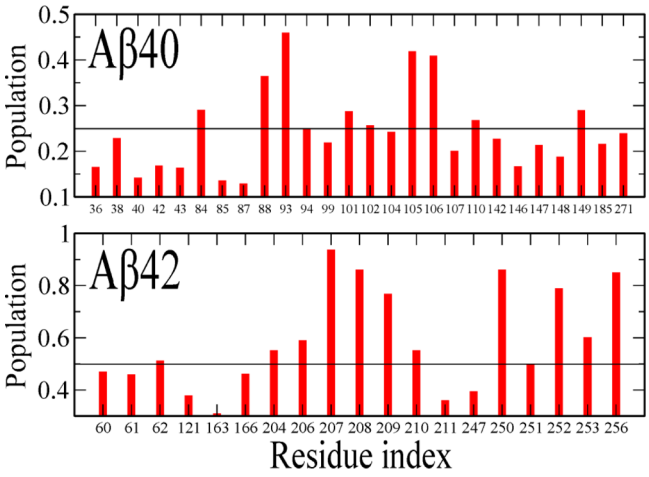

Figure 5. Per-residue distribution of the SC contacts of caspase-3. The residues that have the population exceeding 0.1 and 0.3 for interactions with Aβ40 and Aβ42, respectively, are shown. Results were obtained using the snapshots collected in the last 20 ns of four MD trajectories. Horizontal lines refer to the population equal to 0.25 and 0.5 for Aβ40 and Aβ42, respectively.

caspase residues for Aβ40 and Aβ42 should be higher than 0.25 and 0.5, respectively. For Aβ40 residues, Glu-84, Lys-88, Arg-93, Arg-101, Asp-102, Lys-105, Glu-106, Lys-110, and Arg-149 are the most active ones. The experimental data also showed that Aβ40 binds to the R79−R93 region of caspase-3. Therefore, this result is consistent with the experimental result showing that Glu-84, Lys-88, and Arg-93 belong to the same binding region. By comparison, Thr-62, Tyr-204, Trp-206, Arg-207, Asn-208, Ser-209, Lys-210, Phe-250, Phe-252, Asp-253, and Phe-256 are active for Aβ42. The population is higher than 50%. The result is also in agreement with the experiment data showing Lys-210 is among these active residues.

DOI: 10.1021/acschemneuro.6b00049
ACS Chem. Neurosci. 2016, 7, 1097−1106

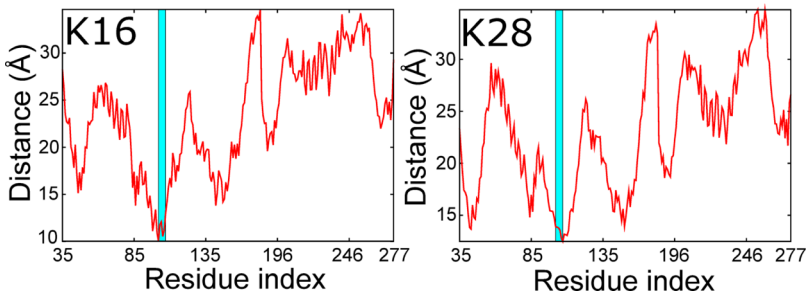

Figure 6. Average distance between the centers of mass of K16 and K28 of Aβ40 and the residues of chain A of caspase-3. K105 of subunit p17 is in the cyan line.

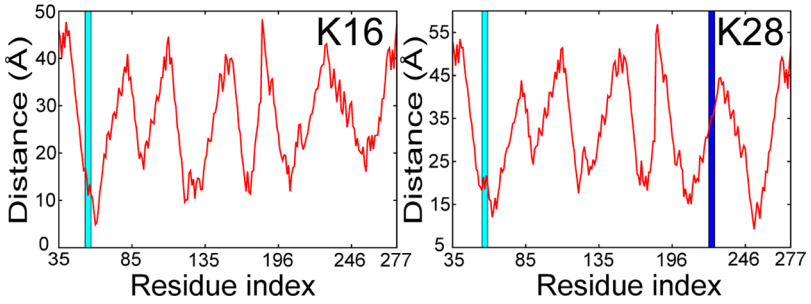

Figure 7. Average distance between the centers of mass of K16 and K28 of Aβ42 and the residues of caspase-3. K53 and K57 of p17 are in the cyan line and K224 of subunit p12 is in the blue line.

Our *in vitro* cross-linking experiment suggested that K16 and K28 of Aβ40 are cross-linked with K105 of the p17 subunit (linkages 1 and 2, respectively). In the Aβ42 case, K16 forms cross-links with K53 and K57 of subunit p17 (linkages 3 and 4, respectively), while K28 is cross-linked with K57 of p17 subunit (linkage 5) and K224 of p12 subunit (linkage 6). To investigate the proximity between K16 and K28 of the Aβ peptides and caspase-3, we calculated the mean distance between the centers of mass of all caspase-3 residues and K16 and K28 of Aβ40 and Aβ42 by using the snapshots collected in the last 20 ns of the four MD trajectories. In Aβ40, K16 and K28 are both in proximity with K105 of p17 (Figure 6). For Aβ42, K16 is in the vicinity of K53 and K57 of p17 (note that K53 and K57 are too close that they belong to the same cyan lane); however, K28 is only close to K57 of p17, but it is far away from K224 of p12 subunit (Figure 7). Considering the approximate nature of the MD simulations, we concluded that the agreement with experimental findings is satisfactory.

Caspase-3, the key executioner of apoptosis, plays a detrimental role in AD. Our study revealed a specific and direct inhibition effect of Aβ on mature caspase-3. We found that freshly prepared Aβ42 species is the most potent species in caspase inhibition among those examined. The hydrophobic C-terminal region plays a key role in the inhibition but the electrostatic interaction is a driving force for association of Aβ monomers with caspase-3. The binding regions of Aβ40 and Aβ42 to caspase-3 were revealed by MD simulations and experimental cross-linking studies. Since Aβ is prone to aggregation, we cannot claim that freshly prepared Aβ species are 100% in their monomeric state. Nevertheless, the level of their oligomers should be much lower than the oligomer preparation in which the peptide was incubated for 1 day. In TEM images (see Supplementary Figure S1), few aggregates were found in the freshly prepared Aβ40 and Aβ42, but spherical oligomers were observed after the oligomer preparation.

Caspase-3 activity is governed by the conserved catalytic motif $QAC_{163}RG$ with the catalytic cysteine residue. Caspase-3 matured from pro-caspase-3 requires precise loop movements to bring key residues into an active position for substrate binding and cleavages. The loops in caspase-3 are loop 1 (L1, 52−66), loop 2 (L2, 163−175, and L2′, 176−192), loop 3 (L3, 198−213), and loop 4 (L4, 247−263).[25] We found that the binding interface of Aβ40 to caspase-3 is located near R79−R93 that is within the first α-helix and the second β-strand of p17 and K105 in close approximation is at the end of the second α-helix of p17. The interacting region is away from the loops and catalytic motif. The binding interface of Aβ42 to caspase-3 is predominantly at K53 and K57 of p17 as well as K224 of p12 subunit. K53 and K57 are located in the L1 region whereas K224 is located at the fourth α-helix of p12. Both interactions revealed that Aβ binding does not occur at the substrate binding site. The result is consistent with our enzymatic assays showing that Aβ is a noncompetitive inhibitor of caspase-3. The manipulation of allosteric sites for caspases is considered as a possible therapeutic strategy.[26] Our study provided a novel binding site of caspase-3 in comparison with other known binding interfaces such as loop binding by BIR-2 to L2[25] and dimer interface binding by small compounds.[26a]

Aβ is a hydrophobic peptide that is prone to aggregate to toxic amyloid species such as oligomers and fibrils. It has been shown that hydrophobic, amyloid-like β-strand peptide sequesters many proteins in cellular compartments.[27] Although many cellular and *in vivo* studies have shown that Aβ treatment leads to apoptosis and caspase-3 activation,[28] the studies have not demonstrated a direct interaction between Aβ and mature caspase-3. Since Aβ treatment triggers calcium influx to cells and leads to apoptosis, we believe that cellular caspase activation after Aβ treatment is through indirect effect. Previously Zorn et al.[21] found that a trace amount of mature caspase-3 processes procaspase-3 more efficiently in the presence of Aβ fibrils.[21] It demonstrated that Aβ fibrils can

DOI: 10.1021/acschemneuro.6b00049
ACS Chem. Neurosci. 2016, 7, 1097−1106

serve as a scaffold for procaspase-3 concentration to facilitate its maturation, but the result did not examine the direct effect of Aβ on mature caspase-3. In fact, many literature supports Aβ monomer to be neuroprotective.[20,29] Aβ42 monomers promote rat cortical neuron survival against trophic deprivation and NMDA toxicity through activating the PI3K pathway.[20] Co-incubation of Aβ40 with cortical neurons, cerebellar granule neurons, and SH-SY5Y cells prevents the toxicity of secretase inhibitor in a dose-dependent manner.[30] Monomeric Aβ40 and Aβ42 are the major forms for synaptic plasticity and neuronal survival.[31] Aβ was also found to be neuroprotective for hypoxia[29a] and as a neurotrophic factor.[29b] Aβ42 was found to regulate presynaptic nicotinic receptors as a presynaptic modulator.[31,32] This evidence may be related to our finding that Aβ directly inhibits caspase-3. Our study showed that freshly prepared Aβ is more effective than oligomers and fibrils to inhibit caspase-3. This finding may suggest a protective role of intracellular Aβ monomer in caspase related pathways including apoptosis in physiological conditions and in AD. Aβ may possibly sequester other caspases for their biological functions since caspase family members, such as initiator caspases, namely caspase-2, -8, -9, and -10, and effector caspases, namely caspase-3, -6, and -7, adopt similar heterodimeric structures. Overall, our study describes a novel mechanism of Aβ and caspase-3 interaction, and the results potentiate future therapeutic development in AD.

METHODS

Materials. Aβ peptides were synthesized via solid-phase peptide synthesis in the peptide synthesis core in Genomics Research Center, Academia Sinica, Taiwan, according to previous literature procedures.[33] Hexafluoro-isopropanol (HFIP), recombinant human active caspase-3, z-DEVD-AFC, and dimethyl sulfoxide (DMSO) were purchased from Sigma-Aldrich (St. Louis, MO, United States).

Aβ Preparation. Full-length Aβ peptides and peptide fragments were dissolved in 100% HFIP at 2.5 mg/mL. HFIP was evaporated in vacuum for >3 h, and Aβ was resuspended by anhydrous DMSO. The final concentration of DMSO for the activity assays was <2%. For freshly prepared Aβ, Aβ was rapidly refolded into assay buffers at indicated concentrations. For Aβ oligomer preparation, Aβ was dissolved in 100% DMSO at 5 mM, refolded into Ham's F12 medium (Caisson Laboratories) at 200 μM, and quiescently incubated at 4 °C for 1 day following a previous literature protocol.[34] For Aβ fibril preparation, Aβ was dissolved in 100% DMSO at 10 mg/mL, refolded in 10 mM sodium phosphate buffer, pH 7.4, at 400 μM, and quiescently incubated at 37 °C for 7 days. The morphology of the species was confirmed by transmission electron microscopy.

Caspase-3 Activity Assay. To monitor caspase-3 activity, the fluorescent caspase-3 substrate, z-DEVD-AFC, was used. The assay buffer contained 50 mM HEPES, pH 7.4, 100 mM NaCl, 10% glycerol, 1 mM EDTA, 0.1% CHAPS, and 10 mM DTT. Aβ samples and the buffer controls were fully dissolved in 78 μL of assay buffer; then, 10 μL of recombinant caspase-3 was mixed in the solution. The solution was transferred to a 96-well ELISA microplate with 90 μL/well. The fluorescence signal was immediately monitored after addition of 10 μL of z-DEVD-AFC solution in a microplate reader, SpectraMax M5 (Molecular Devices, Sunnyvale, CA, United States), with excitation and emission wavelength at 405 and 500 nm, respectively. The final concentration of recombinant caspase-3 and z-DEVD-AFC were 0.1 nM and 200 μM, respectively, or 0.1 μM and 200 μM, respectively. Final Aβ concentrations were indicated. Caspase-3 activity, V_0, was calculated on the basis of the slope of fluorescence signal. Triple replicates of the experiments were performed, and the data were normalized to the caspase-3 activity without Aβ addition. The average values and standard deviations were plotted against Aβ concentration. For Eadie–Hofstee and double reciprocal plots, the z-DEVD-AFC concentration was varied to 120, 50, 25, 16, 12.5, and 10 μM in the assay. For K_i measurement, caspase-3 activity was measured in the presence of various concentrations of Aβ31–42(160, 120, 100, and 0 μM), and each experiment was performed under 100, 50, and 25 μM of caspase-3 substrate. The data of each group were linearly fitted, and K_i value was calculated and averaged from intercepts of the x-axis.

Tryptic Digestion and LC/MS/MS. Caspase-3 alone, Aβ40 or Aβ42 alone, and caspase-3 and Aβ complex were prepared at 10 μM each. The cross-linking was performed by BS3 cross-linker as previously described. DTT at 200 mM (Amresco, United States) and iodoacetamide at 200 mM (Sigma-Aldrich, USA) were freshly prepared in 25 mM ammonium bicarbonate. The samples were mixed with analytical grade trypsin with the weight ratio of 20:1 and incubated at 37 °C for 30 min. The sample was denatured by adding 1 μL of DTT and incubated at 95 °C for 10 min. Alkylation was then performed by further adding 4 μL of iodoacetamide solution. The samples were incubated in the dark at room temperature for 30 min. Alkylation was stopped by adding 4 μL of DTT solution. The sample was concentrated in a speed vacuum concentrator and subjected to LC/MS/MS. The tryptic digestion results were analyzed by software MassMatrix database search engine (http://www.massmatrix.net), and the cross-linked residues were analyzed by the open software MassMatrix database search engine (http://www.massmatrix.net).

Molecular Structures. The structure of caspase-3 was obtained from PDB with PDB ID 1CP3. This protein contains chain A (residues 35–173 and 185–277) and chain B (residues 35–173 and 185–277). Note that chain A is symmetric to chain B. Each chain comprises two subunits, p17 (residues 35–173) and p12 (residues 185–277). Because Aβ40 and Aβ42 monomers are intrinsically disordered in an aqueous environment, their structures were not resolved by the experiment. Therefore, their representative structures were obtained from MD simulations[35] (Supplementary Figure S8). A total of 14 and 25 representatives for Aβ40 (left) and Aβ42 (right), respectively, were collected.

Protein–Protein Docking Simulation. We used HADDOCK server[36] to dock Aβ peptides to caspase-3. In this server, it separates the proteins into active and passive residues. The active residues directly involve the interaction and the passive residues are surrounding surface residues. Based on the experimental results of cross-linking, we found the active residues of caspase-3 that belong to its binding site. In interaction with Aβ40, the active residues are the region R79-R93 of subunit p17, while in the case of Aβ42, only K210 from the p12 subunit is the active residue. All residues of Aβ peptides are the active residues. The protein–protein docking was performed based on these experimental constraints for caspase-3 binding sites, which are supposed to provide reliable results.

MD Simulation. Considering that the predictive power of docking is limited by omission of protein dynamics, we refined the docking results by all-atom MD simulations performed by Gromacs 4.5.5 package with the Amber99SB force field[37] and water model TIP3P.[38] The caspase–Aβ peptide complex obtained in the best docking mode was solvated in a cubic box with periodic boundary conditions and then neutralized by adding counterions. An energy minimization of 100 ps was performed to relieve unfavorable interactions. A MD simulation of 200 ps was subsequently carried out in the NVT ensemble to relax the system (T = 300 K). The production run was performed in the NPT ensemble, with P = 1 bar and T = 300 K. The long-range electrostatic interactions were treated with the particle mesh Ewald (PME) method using 1.4 nm cutoff. The same cutoff was employed for the Lennard-Jones interaction. The pair list was updated every five MD steps, and 40 ns MD simulations were performed. We monitored the change in total energy over time and RMSD from the initial structure to assess the equilibration. The snapshots collected every 10 ps in equilibrium were used for data analysis.

MM-PBSA Method. We applied the MM-PBSA method[38] to estimate the binding free energy of Aβ peptides to caspase-3. The details of this method are presented in our previous studies.[23] In the MM-PBSA approach, the binding free energy of ligand to receptor is defined as follows:

$$\Delta G_{\text{bind}} = \Delta E_{\text{elec}} + \Delta E_{\text{vdW}} + \Delta G_{\text{sur}} + \Delta G_{\text{PB}} - T\Delta S \quad (1)$$

DOI: 10.1021/acschemneuro.6b00049
ACS Chem. Neurosci. 2016, 7, 1097–1106

where ΔE_{elec} and ΔE_{vdW} are contributions from electrostatic and vdW interactions, respectively. ΔG_{sur} and ΔG_{PB} are nonpolar and polar solvation energies, respectively. The entropic contribution $T\Delta S$ is estimated by using the normal mode approximation. The snapshots collected in equilibrium are used to compute the binding free energy expressed by eq 1.

Measures Used in Data Analysis. The side chain contact is accepted when the distance of the center of mass between two residues of caspase-3 and Aβ is ≤6.5 Å. A hydrogen bond is formed if the distance between donor D and acceptor A is ≤3.5 Å and the angle D−H−A is ≥135°.

■ ASSOCIATED CONTENT

Supporting Information

The Supporting Information is available free of charge on the ACS Publications website at DOI: 10.1021/acschemneuro.6b00049.

Methods and results for TEM images of Aβ conformers, Aβ titration to AFC, caspase activity in the presence of aprotinin and RNase A, Aβ effect on GBA and GLA, cell-based caspase-3 activity assay, colocalization of Aβ and caspase-3 in brain slides, fragmentation spectra of cross-linked Aβ and caspase-3, and docking models and analysis (PDF)

■ AUTHOR INFORMATION

Corresponding Authors

* Mai Suan Li. E-mail: masli@ifpan.edu.pl.

*Yun-Ru Chen. E-Mail: yrchen@gate.sinica.edu.tw. Tel: 886-2-2787-1275. Fax: 886-2-2789-8771.

Author Contributions

Y.-J.C. and N.H.L. contributed equally to this work. Y.J.C. performed all experiments except for immunofluorescence staining of mouse tissue, and N.H.L. performed all *in silico* studies. Y.H.S. performed animal study and immunofluorescence tissue staining. H.M.Y. synthesized Aβ peptides. Y.J.C, N.H.L., M.S.L., and Y.R.C. analyzed the data and wrote the manuscript. M.S.L. and Y.R.C. conducted the research.

Funding

The work was funded by National Science Council, Taiwan (Grants NSC 101-2320-B-001-035, NSC 102-2113-M-001-011, and MOST 103-2113-M-001-015), and Department of Science and Technology at Ho Chi Minh City, Vietnam.

Notes

The authors declare no competing financial interest.

■ ACKNOWLEDGMENTS

We thank the peptide synthesis core in the Genomics Research Center for peptide synthesis, the mass spectrometry core for assisting with LC/MS/MS, and the confocal microscope facility in the Genomics Research Center for fluorescence imaging.

■ ABBREVIATIONS

Aβ, amyloid-β; AD, Alzheimer's disease; APP, amyloid precursor protein; aa, amino acids; MD, molecular dynamics; TEM, transmission electron microscopy; RNase A, ribonuclease A; LC/MS/MS, liquid chromatography−tandem mass spectrometry; SC, side chain; HB, hydrogen bonds; RMSD, root-mean-square displacement; vdW, van der Waals; HFIP, hexafluoro-isopropanol; DMSO, dimethyl sulfoxide; PME, particle mesh Ewald; z-DEVD-AFC, *Z*-Asp-Glu-Val-Asp-7-amino-4-trifluoromethylcoumarin, fluorogenic substrate for caspase-3; HEPES, 4-(2-hydroxyethyl)-1-piperazineethanesulfonic acid; EDTA, ethylenediaminetetraacetic acid; CHAPS, 3-[(3-cholamidopropyl)dimethylammonio]-1-propanesulfonate; DTT, dithiothreitol; ELISA, enzyme-linked immunosorbent assay; MM-PBSA, molecular mechanics Poisson−Boltzmann surface area

■ REFERENCES

(1) (a) Roth, M., Tomlinson, B. E., and Blessed, G. (1966) Correlation between Scores for Dementia and Counts of 'Senile Plaques' in Cerebral Grey Matter of Elderly Subjects. *Nature 209* (5018), 109−110. (b) Kang, J., Lemaire, H.-G., Unterbeck, A., Salbaum, J. M., Masters, C. L., Grzeschik, K.-H., Multhaup, G., Beyreuther, K., and Muller-Hill, B. (1987) The precursor of Alzheimer's disease amyloid A4 protein resembles a cell-surface receptor. *Nature 325* (6106), 733−736.

(2) Hardy, J., and Selkoe, D. J. (2002) The amyloid hypothesis of Alzheimer's disease: progress and problems on the road to therapeutics. *Science 297* (5580), 353−6.

(3) (a) Roychaudhuri, R., Yang, M., Hoshi, M. M., and Teplow, D. B. (2009) Amyloid beta-protein assembly and Alzheimer disease. *J. Biol. Chem. 284* (8), 4749−4753. (b) Haass, C., and Selkoe, D. J. (2007) Soluble protein oligomers in neurodegeneration: lessons from the Alzheimer's amyloid beta-peptide. *Nat. Rev. Mol. Cell Biol. 8* (2), 101−12. (c) Dahlgren, K. N., Manelli, A. M., Stine, W. B., Jr., Baker, L. K., Krafft, G. A., and LaDu, M. J. (2002) Oligomeric and fibrillar species of amyloid-beta peptides differentially affect neuronal viability. *J. Biol. Chem. 277* (35), 32046−53. (d) Ahmed, M., Davis, J., Aucoin, D., Sato, T., Ahuja, S., Aimoto, S., Elliott, J. I., Van Nostrand, W. E., and Smith, S. O. (2010) Structural conversion of neurotoxic amyloid-beta(1−42) oligomers to fibrils. *Nat. Struct. Mol. Biol. 17* (5), 561−7.

(4) Chen, Y. R., and Glabe, C. G. (2006) Distinct early folding and aggregation properties of Alzheimer amyloid-beta peptides Abeta40 and Abeta42: stable trimer or tetramer formation by Abeta42. *J. Biol. Chem. 281* (34), 24414−22.

(5) Lazo, N. D., Grant, M. A., Condron, M. C., Rigby, A. C., and Teplow, D. B. (2005) On the nucleation of amyloid beta-protein monomer folding. *Protein Sci. 14* (6), 1581−96.

(6) Hou, L., Shao, H., Zhang, Y., Li, H., Menon, N. K., Neuhaus, E. B., Brewer, J. M., Byeon, I. J., Ray, D. G., Vitek, M. P., Iwashita, T., Makula, R. A., Przybyla, A. B., and Zagorski, M. G. (2004) Solution NMR studies of the A beta(1−40) and A beta(1−42) peptides establish that the Met35 oxidation state affects the mechanism of amyloid formation. *J. Am. Chem. Soc. 126* (7), 1992−2005.

(7) Fradinger, E. A., Monien, B. H., Urbanc, B., Lomakin, A., Tan, M., Li, H., Spring, S. M., Condron, M. M., Cruz, L., Xie, C. W., Benedek, G. B., and Bitan, G. (2008) C-terminal peptides coassemble into Abeta42 oligomers and protect neurons against Abeta42-induced neurotoxicity. *Proc. Natl. Acad. Sci. U. S. A. 105* (37), 14175−80.

(8) (a) Yu, L., Edalji, R., Harlan, J. E., Holzman, T. F., Lopez, A. P., Labkovsky, B., Hillen, H., Barghorn, S., Ebert, U., Richardson, P. L., Miesbauer, L., Solomon, L., Bartley, D., Walter, K., Johnson, R. W., Hajduk, P. J., and Olejniczak, E. T. (2009) Structural characterization of a soluble amyloid beta-peptide oligomer. *Biochemistry 48* (9), 1870−7. (b) Tycko, R. (2006) Molecular structure of amyloid fibrils: insights from solid-state NMR. *Q. Rev. Biophys. 39* (1), 1−55.

(9) Xiao, Y., Ma, B., McElheny, D., Parthasarathy, S., Long, F., Hoshi, M., Nussinov, R., and Ishii, Y. (2015) Abeta(1−42) fibril structure illuminates self-recognition and replication of amyloid in Alzheimer's disease. *Nat. Struct. Mol. Biol. 22* (6), 499−505.

(10) Su, J. H., Anderson, A. J., Cummings, B. J., and Cotman, C. W. (1994) Immunohistochemical evidence for apoptosis in Alzheimer's disease. *NeuroReport 5* (18), 2529−33.

(11) Satou, T., Cummings, B. J., and Cotman, C. W. (1995) Immunoreactivity for Bcl-2 protein within neurons in the Alzheimer's disease brain increases with disease severity. *Brain Res. 697* (1−2), 35−43.

DOI: 10.1021/acschemneuro.6b00049
ACS Chem. Neurosci. 2016, 7, 1097−1106

(12) Loo, D. T., Copani, A., Pike, C. J., Whittemore, E. R., Walencewicz, A. J., and Cotman, C. W. (1993) Apoptosis is induced by beta-amyloid in cultured central nervous system neurons. *Proc. Natl. Acad. Sci. U. S. A. 90* (17), 7951−7955.
(13) (a) Paradis, E., Douillard, H., Koutroumanis, M., Goodyer, C., and LeBlanc, A. (1996) Amyloid β Peptide of Alzheimer's Disease Downregulates Bcl-2 and Upregulates Bax Expression in Human Neurons. *J. Neurosci. 16* (23), 7533−7539. (b) Estus, S., Tucker, H. M., van Rooyen, C., Wright, S., Brigham, E. F., Wogulis, M., and Rydel, R. E. (1997) Aggregated Amyloid-β Protein Induces Cortical Neuronal Apoptosis and Concomitant "Apoptotic" Pattern of Gene Induction. *J. Neurosci. 17* (20), 7736−7745. (c) Kudo, W., Lee, H. P., Smith, M. A., Zhu, X., Matsuyama, S., and Lee, H. g. (2012) Inhibition of Bax protects neuronal cells from oligomeric A[beta] neurotoxicity. *Cell Death Dis. 3*, e309.
(14) (a) D'Amelio, M., Sheng, M., and Cecconi, F. (2012) Caspase-3 in the central nervous system: beyond apoptosis. *Trends Neurosci. 35* (11), 700−9. (b) Hyman, B. T., and Yuan, J. (2012) Apoptotic and non-apoptotic roles of caspases in neuronal physiology and pathophysiology. *Nat. Rev. Neurosci. 13* (6), 395−406.
(15) (a) LaFerla, F. M., Green, K. N., and Oddo, S. (2007) Intracellular amyloid-beta in Alzheimer's disease. *Nat. Rev. Neurosci. 8* (7), 499−509. (b) Pensalfini, A., Albay, R., 3rd, Rasool, S., Wu, J. W., Hatami, A., Arai, H., Margol, L., Milton, S., Poon, W. W., Corrada, M. M., Kawas, C. H., and Glabe, C. G. (2014) Intracellular amyloid and the neuronal origin of Alzheimer neuritic plaques. *Neurobiol. Dis. 71*, 53−61.
(16) Gouras, G. K., Tsai, J., Naslund, J., Vincent, B., Edgar, M., Checler, F., Greenfield, J. P., Haroutunian, V., Buxbaum, J. D., Xu, H., Greengard, P., and Relkin, N. R. (2000) Intraneuronal Abeta42 accumulation in human brain. *Am. J. Pathol. 156* (1), 15−20.
(17) Takahashi, R. H., Milner, T. A., Li, F., Nam, E. E., Edgar, M. A., Yamaguchi, H., Beal, M. F., Xu, H., Greengard, P., and Gouras, G. K. (2002) Intraneuronal Alzheimer abeta42 accumulates in multivesicular bodies and is associated with synaptic pathology. *Am. J. Pathol. 161* (5), 1869−79.
(18) Billings, L. M., Oddo, S., Green, K. N., McGaugh, J. L., and LaFerla, F. M. (2005) Intraneuronal A^2 Causes the Onset of Early Alzheimer s Disease-Related Cognitive Deficits in Transgenic Mice. *Neuron 45* (5), 675−688.
(19) Cataldo, A. M., Petanceska, S., Terio, N. B., Peterhoff, C. M., Durham, R., Mercken, M., Mehta, P. D., Buxbaum, J., Haroutunian, V., and Nixon, R. A. (2004) Aβ localization in abnormal endosomes: association with earliest Aβ elevations in AD and Down syndrome. *Neurobiol. Aging 25* (10), 1263−1272.
(20) Giuffrida, M. L., Caraci, F., Pignataro, B., Cataldo, S., De Bona, P., Bruno, V., Molinaro, G., Pappalardo, G., Messina, A., Palmigiano, A., Garozzo, D., Nicoletti, F., Rizzarelli, E., and Copani, A. (2009) Beta-amyloid monomers are neuroprotective. *J. Neurosci. 29* (34), 10582−7.
(21) Zorn, J. A., Wolan, D. W., Agard, N. J., and Wells, J. A. (2012) Fibrils Colocalize Caspase-3 with Procaspase-3 to Foster Maturation. *J. Biol. Chem. 287* (40), 33781−33795.
(22) Chang, Y. J., and Chen, Y. R. (2014) The coexistence of an equal amount of Alzheimer's amyloid-beta 40 and 42 forms structurally stable and toxic oligomers through a distinct pathway. *FEBS J. 281* (11), 2674−87.
(23) (a) Nguyen, T. T., Mai, B. K., and Li, M. S. (2011) Study of Tamiflu sensitivity to variants of A/H5N1 virus using different force fields. *J. Chem. Inf. Model. 51* (9), 2266−76. (b) Ngo, S. T., and Li, M. S. (2012) Curcumin binds to Abeta1−40 peptides and fibrils stronger than ibuprofen and naproxen. *J. Phys. Chem. B 116* (34), 10165−75.
(24) Viet, M. H., Siposova, K., Bednarikova, Z., Antosova, A., Nguyen, T. T., Gazova, Z., and Li, M. S. (2015) In Silico and in Vitro Study of Binding Affinity of Tripeptides to Amyloid beta Fibrils: Implications for Alzheimer's Disease. *J. Phys. Chem. B 119* (16), 5145−55.
(25) MacKenzie, S. H., and Clark, A. C. (2008) Targeting cell death in tumors by activating caspases. *Curr. Cancer Drug Targets 8* (2), 98−109.
(26) (a) Feldman, T., Kabaleeswaran, V., Jang, S. B., Antczak, C., Djaballah, H., Wu, H., and Jiang, X. (2012) A class of allosteric caspase inhibitors identified by high-throughput screening. *Mol. Cell 47* (4), 585−95. (b) Stanger, K., Steffek, M., Zhou, L., Pozniak, C. D., Quan, C., Franke, Y., Tom, J., Tam, C., Elliott, J. M., Lewcock, J. W., Zhang, Y., Murray, J., and Hannoush, R. N. (2012) Allosteric peptides bind a caspase zymogen and mediate caspase tetramerization. *Nat. Chem. Biol. 8* (7), 655−60. (c) Cade, C., Swartz, P., MacKenzie, S. H., and Clark, A. C. (2014) Modifying caspase-3 activity by altering allosteric networks. *Biochemistry 53* (48), 7582−95.
(27) Olzscha, H., Schermann, S. M., Woerner, A. C., Pinkert, S., Hecht, M. H., Tartaglia, G. G., Vendruscolo, M., Hayer-Hartl, M., Hartl, F. U., and Vabulas, R. M. (2011) Amyloid-like aggregates sequester numerous metastable proteins with essential cellular functions. *Cell 144* (1), 67−78.
(28) Hyman, B. T. (2011) Caspase activation without apoptosis: insight into Abeta initiation of neurodegeneration. *Nat. Neurosci. 14* (1), 5−6.
(29) (a) Pearson, H. A., and Peers, C. (2006) Physiological roles for amyloid β peptides. *J. Physiol. 575*, 5−10. (b) Giuffrida, M. L., Tomasello, M. F., Pandini, G., Caraci, F., Battaglia, G., Busceti, C., Di Pietro, P., Pappalardo, G., Attanasio, F., Chiechio, S., Bagnoli, S., Nacmias, B., Sorbi, S., Vigneri, R., Rizzarelli, E., Nicoletti, F., and Copani, A. (2015) Monomeric β-amyloid interacts with type-1 insulin-like growth factor receptors to provide energy supply to neurons. *Front. Cell. Neurosci. 9*, 297.
(30) Plant, L. D., Boyle, J. P., Smith, I. F., Peers, C., and Pearson, H. A. (2003) The production of amyloid beta peptide is a critical requirement for the viability of central neurons. *J. Neurosci. 23* (13), 5531−5.
(31) Parihar, M. S., and Brewer, G. J. (2010) Amyloid-beta as a modulator of synaptic plasticity. *J. Alzheimers Dis 22* (3), 741−63.
(32) Dougherty, J. J., Wu, J., and Nichols, R. A. (2003) β-Amyloid Regulation of Presynaptic Nicotinic Receptors in Rat Hippocampus and Neocortex. *J. Neurosci. 23* (17), 6740−6747.
(33) Burdick, D., Soreghan, B., Kwon, M., Kosmoski, J., Knauer, M., Henschen, A., Yates, J., Cotman, C., and Glabe, C. (1992) Assembly and aggregation properties of synthetic Alzheimer's A4/beta amyloid peptide analogs. *J. Biol. Chem. 267* (1), 546−54.
(34) Stine, W. B., Jr., Dahlgren, K. N., Krafft, G. A., and LaDu, M. J. (2003) In vitro characterization of conditions for amyloid-beta peptide oligomerization and fibrillogenesis. *J. Biol. Chem. 278* (13), 11612−22.
(35) (a) Yang, M., and Teplow, D. B. (2008) Amyloid beta-protein monomer folding: free-energy surfaces reveal alloform-specific differences. *J. Mol. Biol. 384* (2), 450−64. (b) Viet, M. H., Nguyen, P. H., Ngo, S. T., Li, M. S., and Derreumaux, P. (2013) Effect of the Tottori familial disease mutation (D7N) on the monomers and dimers of Abeta40 and Abeta42. *ACS Chem. Neurosci. 4* (11), 1446−57.
(36) de Vries, S. J., van Dijk, M., and Bonvin, A. M. (2010) The HADDOCK web server for data-driven biomolecular docking. *Nat. Protoc. 5* (5), 883−97.
(37) Hornak, V., Abel, R., Okur, A., Strockbine, B., Roitberg, A., and Simmerling, C. (2006) Comparison of multiple Amber force fields and development of improved protein backbone parameters. *Proteins: Struct., Funct., Genet. 65* (3), 712−25.
(38) Jorgensen, W. L., Chandrasekhar, J., Madura, J. D., Impey, R. W., and Klein, M. L. (1983) Comparison of Simple Potential Functions for Simulating Liquid Water. *J. Chem. Phys. 79* (2), 926−935.

DOI: 10.1021/acschemneuro.6b00049
ACS Chem. Neurosci. 2016, 7, 1097−1106